Proteomic Profiling of Leukocytes Reveals Dysregulation of Adhesion and Integrin Proteins in Chronic Kidney Disease-Related Atherosclerosis

Tracz, Joanna

2021-06-04

Tracz , J , Handschuh , L , Lalowski , M , Marczak , L , Kostka-Jeziorny , K , Perek , B , Wanic-Kossowska , M , Podkowinska , A , Tykarski , A , Formanowicz , D & Luczak , M 2021 , ' Proteomic Profiling of Leukocytes Reveals Dysregulation of Adhesion and Integrin Proteins in Chronic Kidney Disease-Related Atherosclerosis ' , Journal of Proteome Research , vol. 20 , no. 6 , pp. 3053-3067 . https://doi.org/10.1021/acs.jproteome.0c00883

http://hdl.handle.net/10138/344287
https://doi.org/10.1021/acs.jproteome.0c00883

publishedVersion

Journal of proteome research

pubs.acs.org/jpr

Article

Proteomic Profiling of Leukocytes Reveals Dysregulation of Adhesion and Integrin Proteins in Chronic Kidney Disease-Related Atherosclerosis

Joanna Tracz, Luiza Handschuh, Maciej Lalowski, Łukasz Marczak, Katarzyna Kostka-Jeziorny, Bartłomiej Perek, Maria Wanic-Kossowska, Alina Podkowińska, Andrzej Tykarski, Dorota Formanowicz, and Magdalena Luczak*

Cite This: *J. Proteome Res.* 2021, 20, 3053−3067

Read Online

ACCESS | Metrics & More | Article Recommendations | Supporting Information

ABSTRACT: A progressive loss of functional nephrons defines chronic kidney disease (CKD). Complications related to cardiovascular disease (CVD) are the principal causes of mortality in CKD; however, the acceleration of CVD in CKD remains unresolved. Our study used a complementary proteomic approach to assess mild and advanced CKD patients with different atherosclerosis stages and two groups of patients with different classical CVD progression but without renal dysfunction. We utilized a label-free approach based on LC-MS/MS and functional bioinformatic analyses to profile CKD and CVD leukocyte proteins. We revealed dysregulation of proteins involved in different phases of leukocytes' diapedesis process that is very pronounced in CKD's advanced stage. We also showed an upregulation of apoptosis-related proteins in CKD as compared to CVD. The differential abundance of selected proteins was validated by multiple reaction monitoring, ELISA, Western blotting, and at the mRNA level by ddPCR. An increased rate of apoptosis was then functionally confirmed on the cellular level. Hence, we suggest that the disturbances in leukocyte extravasation proteins may alter cell integrity and trigger cell death, as demonstrated by flow cytometry and microscopy analyses. Our proteomics data set has been deposited to the ProteomeXchange Consortium via the PRIDE repository with the data set identifier PXD018596.

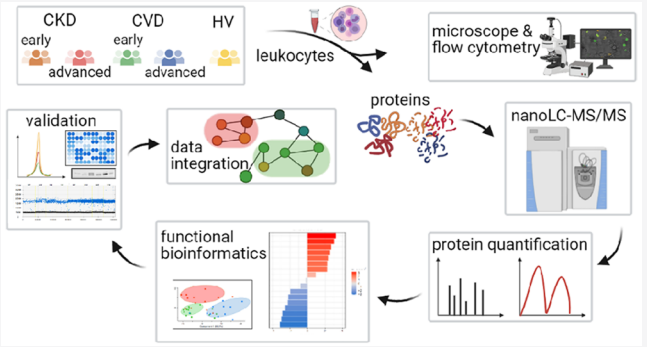

KEYWORDS: *chronic kidney disease, cardiovascular disease, adhesion, integrin, proteomics, mass spectrometry*

1. INTRODUCTION

Chronic kidney disease (CKD) is a global health problem with a constantly enhancing rate, defined and categorized by a progressive loss of functional nephrons resulting in a gradual reduction of glomerular filtration rate (GFR) and proteinuria.[1] However, not an impaired kidney function *per se*, but accelerated atherosclerosis followed by cardiovascular disease (CVD) complications represent the principal causes of mortality in CKD.[2] The severity of CVD in CKD increases along with renal damage progression;[3] hence, patients with kidney failure often demonstrate even a 20-fold increase in cardiovascular mortality risk than in the general population.[4] The vast majority of CKD patients succumb to cardiovascular death prior to developing kidney failure.[5]

Interestingly, in marked contrast to the general population, well-established risk factors, like hypertension, high serum cholesterol level, or obesity, appear to be associated with markedly higher survival rates in CKD. These paradoxical observations have been termed as "reverse epidemiology" and disclose that traditionally recognized risk factors might inadequately explain the high incidence of CVD in CKD patients.[6] It has also been demonstrated that other risk factors, including endothelial dysfunction, vascular calcification, volume overload, oxidative stress, and inflammation, may play a key role in the high incidence of CVD risk in CKD. This issue seems to be of vital importance; however, due to many confounding factors, patients with CKD are often excluded from CVD-oriented studies, which limits the understanding of their high-risk, CKD-related atherosclerosis.[7]

It should be emphasized that CKD is currently treated as an oxidative stress- and inflammatory-mediated CVD, underlined by accelerated atherosclerosis (for a review, see ref 8). This phenomenon is very complex; thus deeper insights into the

Received: November 4, 2020
Published: May 3, 2021

Table 1. Characteristics of the Study Population[a]

	group						
	HV	CKD1-2	CKD5	CVD1	CVD2	*p*-value	*p*-value without HVs
age [years]	43 ± 6	66 ± 8	65 ± 17	62 ± 15	63 ± 9	<0.0001	0.25
male/female	16/8	18/8	18/9	17/10	16/6	0.92	0.86
BMI [kg/m^2]	24 ± 2	29 ± 4	25 ± 3	29 ± 5	26 ± 4	0.13	0.33
obesity (BMI > 30 kg/m^2)	0	3	0	4	1	<0.0001	<0.0001
arterial hypertension	0	26	27	27	22	<0.0001	1.00
hyperlipidemia	0	26	2	27	22	<0.0001	<0.0001
CAD/previous myocardial infarction	0/0	0/0	27/15	0/0	22/17	<0.0001	<0.0001
previous PCI	0	0	18	0	22	<0.0001	<0.0001
PVD	0	0	2	0	4	<0.0001	<0.0001
neurological events	0	0	1	0	4	<0.0001	<0.0001
eGFR [mL/min/1.73 m^2]	95.3 ± 13.9	68.0 ± 5.1	8.5 ± 3.9	106.4 ± 13.4	90.7 ± 10.7	<0.0001	<0.0001
glucose [mM]	4.0 ± 0.6	5.4 ± 0.4	5.6 ± 0.4	5.5 ± 0.5	5.1 ± 0.3	0.02	0.07
total cholesterol [mg/dL]	190.5 ± 23.9	170.8 ± 50.1	157.2 ± 29.3	189 ± 92	175 ± 37	0.01	0.10
HDL cholesterol [mg/dL]	50.3 ± 13.1	63.8 ± 20.1	45.7 ± 11.7	65.1 ± 17.8	56.3 ± 12.8	<0.0001	<0.0001
LDL cholesterol [mg/dL]	123.0 ± 2	87.5 ± 44.2	84.4 ± 28.9	102.2 ± 47	95.8 ± 29.8	<0.0001	0.38
triglycerides [mg/dL]	91.3 ± 41.0	103.6 ± 41.1	135.7 ± 77.4	131.3 ± 93.1	113.0 ± 41.3	0.23	0.73
hsCRP [mg/L]	1.7 ± 1.9	2.4 ± 2.3	22.2 ± 29.8	2.3 ± 1.9	2.2 ± 3.0	<0.0001	<0.0001
WBC [10^9/L]	6.1 ± 1.5	7.2 ± 2.4	7.1 ± 2.4	6.9 ± 2.4	8.8 ± 6.7	0.44	0.91
NEUT [10^9/L]	3.2 ± 1.0	4.5 ± 1.7	4.6 ± 2	4.3 ± 2.2	4.3 ± 1.1	0.04	0.88
EOS [10^9/L]	0.18 ± 0.1	0.18 ± 0.13	0.22 ± 0.14	0.1 ± 0.1	0.13 ± 0.04	0.11	0.16
BASO [10^9/L]	0.03 ± 0.01	0.03 ± 0.02	0.03 ± 0.23	0.03 ± 0.01	0.03 ± 0.02	0.97	0.81
LYMPH [10^9/L]	2.1 ± 0.6	1.9 ± 0.5	1.4 ± 0.8	1.7 ± 0.6	1.9 ± 0.6	<0.0001	0.12
MONO [10^9/L]	0.4 ± 0.1	0.4 ± 0.2	0.7 ± 0.2	0.4 ± 0.1	0.4 ± 0.1	<0.0001	<0.0001
RBC [10^{12}/L]	4.5 ± 0.4	4.7 ± 0.4	3.2 ± 0.5	4.5 ± 0.4	4.8 ± 1.2	<0.0001	<0.0001
PLT [10^9/L]	262.1 ± 78.5	243.9 ± 87.9	205.0 ± 65.8	249.8 ± 54.2	236 ± 78.5	0.01	0.02
antiplatelet treatment	0	21	19	18	18	<0.0001	0.51
acetylsalicylic acid	0	18	12	15	16	<0.0001	0.11
acetylsalicylic acid + ticagrelor	0	2	3	2	1	<0.0001	0.86
acetylsalicylic acid + clopidogrel	0	1	3	1	1	<0.0001	0.61
hypertension treatment	0	26	27	27	22	<0.0001	1.00
β-blocker	0	18	16	19	18	<0.0001	0.40
diuretics	0	13	13	12	13	<0.0001	0.91
ACEI	0	18	2	14	2	<0.0001	<0.0001
CCB	0	6	11	7	6	<0.0001	0.50
ARB	0	4	2	5	2	<0.0001	0.59
statin (atorvastatin or rosuvastatin)	0	23	17	19	22	<0.0001	0.02

[a]Mean value ± SD. Abbreviations: HV, healthy volunteer; BMI, body mass index; CAD, coronary artery disease; PCI, percutaneous coronary interventions; PVD, peripheral vascular disease; eGFR, estimated glomerular filtration rate; hsCRP, high-sensitivity C-reactive protein; WBC, white blood cells; EOS, eosinophils; BASO, basophils; LYMPH, lymphocytes; MONO, monocytes; RBC, red blood cells; PLT, platelets; ACE, angiotensin-converting enzyme inhibitors; CCB, calcium channel blocker; ARB, angiotensin receptor blocker. The chi-square test was used for categorical variables (gender, drug treatment, the prevalence of hypertension, obesity, hyperlipidemia, CAD, PCI, PVD, and events). For other variables, the Mann−Whitney U-test was used.

relationships between the many disrupted metabolic pathways involved in CKD pathology are strongly recommended.

Although the close connection between kidney dysfunction and atherosclerosis is widely recognized, almost all existing studies rely on comparing CKD or CVD patients separately to healthy controls. Therefore, only direct analysis of both conditions may provide information about the differences underlying atherosclerotic CVD related and non-related to CKD.

Since atherosclerosis is regulated by a complex interplay of circulating plasma proteins and inflammatory cells, and soluble forms of these molecules could be detected in plasma, the analysis of a repertoire of constitutive proteins in leukocytes during CKD-related atherosclerosis progression could be critical. Many proteomic studies presenting alterations in plasma protein profiles from patients with either CKD or CVD have previously been published.[9,10] We earlier presented a comparative proteomic analysis of plasma from CKD and CVD patients and demonstrated that proteins involved in inflammation exhibited more significant alterations in individuals with CKD-related atherosclerosis.[11]

In this study, we utilized a label-free proteomics approach to increase our knowledge about the alteration of leukocyte proteins in CKD and CVD. We aimed to assess mild and advanced CKD patients with different CKD-related atherosclerosis progression and two groups of CVD patients with non-CKD-related atherosclerosis. The obtained results were confirmed by ELISA, digital droplet PCR (ddPCR), and

https://doi.org/10.1021/acs.jproteome.0c00883
J. Proteome Res. 2021, 20, 3053−3067

multiple reaction monitoring (MRM). Cells were subsequently evaluated by microscopy and flow cytometry, and then functionally analyzed by a network approach. Measurements of adhesion molecules with a known role in atherosclerosis development and circulating in plasma were also performed to validate selected findings.

2. MATERIAL AND METHODS

2.1. Experimental Groups and Sample Preparation

The study protocol conformed to the Ethical Guidelines of the World Medical Association Declaration of Helsinki. Before the project commenced, appropriate approval was obtained from the Bioethical Commission of the Poznan University of Medical Sciences, Poland (no. 926/16). All patients qualified for this study underwent a clinical examination and provided signed informed consent before participation. The study involved 220 patients divided into four experimental groups (named CKD1-2, CKD5, CVD1, and CVD2, respectively) and 48 healthy volunteers. During 2016−2017, samples were collected from dialysis stations and Poznan University of Medical Sciences' four clinical departments.

The CKD patients were divided into two groups based on NICE Clinical Guidelines[12] and according to their levels of eGFR.[13] The first group, named CKD1-2, encompassed patients at the initial stage of CKD with a mean eGFR of 68 mL/min/1.73 m^2. The second CKD group, called CKD5, included ESRD patients treated with hemodialysis, mean eGFR of 8.5 mL/min/1.73 m^2. The study was also carried out on two groups of CVD patients varying in the degree of CVD clinical manifestation (CVD1 and CVD2) but without kidney dysfunction and thus eGFR > 90 mL/min/1.73 m^2.

The CKD1-2 and CVD1 groups included patients with no previous cardiovascular events and vascular interventions; they were burdened with commonly accepted risk factors of atherosclerosis development, i.e., hypertension and hyperlipidemia, with non-obstructive coronary artery disease (non-hemodynamically significant stenosis less than 30%) confirmed by coronarography. Both groups differed only in kidney function.

Patients comprising the CVD2 and CKD5 groups had advanced atherosclerosis, confirmed by coronarography clinically manifested as coronary artery disease (CAD) with a history of at least one acute coronary syndrome and/or after the vascular intervention. Again, only kidney function differentiated these groups. Thus, the following groups were involved in this study:

(I) Group CVD1 - normal kidney function; hypertension, hyperlipidemia, and non-obstructive coronary artery disease
(II) Group CVD2 - normal kidney function; symptomatic CVD
(III) Group CKD1-2 - an early stage of kidney disease; hypertension, hyperlipidemia, and non-obstructive coronary artery disease
(IV) Group CKD5 - severe kidney disease; symptomatic CVD

All patient groups were examined by coronarography, echocardiography, electrocardiography, and Doppler ultrasonography. The characteristics of all experimental groups are presented in Table 1.

The set exclusion criteria for patients included diabetes, active acute infection, and malignant tumors. In order to avoid problems associated with different treatments, patient groups were also matched concerning types of statins used and hypertension and antiplatelet drugs. Patients treated with anticoagulants were also excluded from the analysis. Ultimately, 126 samples were selected for LC-MS analyses performed in triplicate.

Blood samples were collected, and at the same time, standard biochemical examinations were performed. In the case of hemodialyzed patients, blood samples were drawn prior to the second hemodialysis session of the week, as recommended. White blood cells were isolated using the RBC lysis solution procedure as described.[14] Plasma samples were also frozen at −80 °C until analysis. The cell pellet containing leukocytes was analyzed by fluorescence microscopy and flow cytometry to assess the morphology, preparation quality, and apoptosis/necrosis rate. Cells were stained with Hoechst 33342 (Thermo Fisher Scientific, Waltham, MA, USA). The rates of apoptotic and necrotic cells were evaluated with dual staining with CellEvent Casp3/7-FITC (Thermo Fisher Scientific, Waltham, MA, USA) according to the manufacturer's protocol and propidium iodide (1.25 μg/mL; Sigma-Aldrich, Milwaukee, WI, USA) fluorescent dyes. The intensity of green fluorescence was analyzed with 488 nm excitation by an Accuri C6 flow cytometer (Becton Dickinson (BD), Franklin Lakes, NJ, USA). Leukocytes were gated by size and granularity to assess particular subpopulations of cells. For confocal microscopy, cells were placed on a glass slide, coverslipped, and analyzed with a Leica TCS SP5 microscope (Leica Microsystems, Wetzlar, Germany) with a Plan Apo 63 × 1.4 NA oil-immersion objective. Sequentially scanned images were collected at Ex/Em = 502/510−550 nm for living cells, 535/610−650 nm for apoptotic cells, and 405/450−500 nm for nuclei staining. Leica LAS AF and Leica LAS X software with a deconvolution module were used for image processing and fluorescence analysis, respectively.

The rest of the leukocytes was aliquoted, frozen, and stored in a vapor phase of liquid N_2 until analysis. For ddPCR analysis, cell pellets were suspended in a mirVana Ambion miRNA Isolation Kit lysis buffer (Thermo Fisher Scientific, Waltham MA, USA) and immediately frozen at −80 °C.

2.2. Protein Preparation and Nano LC-MS/MS Analysis

The cell pellets of leukocytes were suspended in 8 M urea/0.2% SDS and homogenized using Precellys24 homogenizer (Bertis Technologies, Villeurbanne, France) in three, 30-s cycles at 5500 rpm. Next, the samples were sonicated on ice for 10 min. Proteins were precipitated with six volumes of cold acetone and then washed with 80% acetone to remove SDS. The protein pellet was resuspended in 25 μL of 50 mM ammonium bicarbonate, vortexed for 1 h at RT, and sonicated for 10 min using an ultrasonic bath. After that, the samples were centrifuged at 23000*g* for 10 min at 4 °C, and the supernatants were used for protein concentration assay (2D-Quant Kit, GE Healthcare, Uppsala, Sweden). A 30 μg portion of the protein mixture was reduced with 5.6 mM DTT for 5 min at 95 °C and then alkylated with 5 mM iodoacetamide for 20 min at RT. The samples were digested with 0.2 μg of trypsin (Promega, Mannheim, Germany) overnight at 37 °C. The peptide mixtures were analyzed by nano-LC-MS/MS using a Dionex UltiMate 3000 RSLCnano System coupled with Q-Exactive Orbitrap mass spectrometer (Thermo Fisher Scientific, Waltham, MA, USA) in one batch as described.[11] Following LC-MS/MS analysis, the raw files were analyzed to

https://doi.org/10.1021/acs.jproteome.0c00883
J. Proteome Res. 2021, 20, 3053−3067

evaluate the quality of the performed runs by Proteome Discoverer (PD), version 1.4.14 (Thermo Fisher Scientific, Waltham, MA, USA), as described.[11] The reproducibility of the biological and technical replicates was assessed by scatter plotting, and the correlation coefficient was determined based on the label-free quantification (LFQ) intensities. Only samples with Pearson correlation coefficients above 0.8 (125 out of 126) were included in quantitative surveys (Table S1).

2.3. Quantitative Analysis of Proteomic Data

The raw files were quantitatively analyzed by MaxQuant (MQ),[15] version 1.5.1.2. The identification of proteins at ≤1% FDR was performed against the UniProt complete human proteome set (release 10-03-2019) using tolerance levels of 10 ppm for MS and 0.08 Da for MS/MS, and two missed cleavages were allowed. The carbamidomethylation of cysteines was set as a fixed modification, and the oxidation of methionine was allowed as a variable modification. The analysis of the samples was based on the LFQ intensities. The normalized MQ data were analyzed with Perseus software, version 1.6.1.3 (https://maxquant.net/perseus/). The MQ data were filtered to exclude false-positive identifications (contaminants, reverse identifications, and proteins "only identified by site"). Only proteins detected in all samples were taken into account in the quantitative analyses (no missing values). The fold changes in the level of the proteins were assessed by comparing the mean intensities among all experimental groups.

2.4. Validation of Results with Quantitative ddPCR

Ten patients' samples from each experimental group were chosen for ddPCR analysis. Total RNA was extracted from the leukocytes with a mirVana miRNA Isolation Kit and DNase-digested with a TURBO DNA-free Kit according to the manufacturers' protocols. RNA quantity was determined using a NanoDrop 2000 spectrophotometer. The quality of RNA was assessed with a Bioanalyzer 2100 with a Total RNA Pico Assay (Agilent Technologies, Santa Clara, USA). RNA (0.5 μg per sample) was used for reverse transcription by SuperScript III RT and oligo(dT) (Thermo Fisher Scientific, Waltham, MA, USA). The reaction mixtures were incubated for 1.5 h at 50 °C. Six pairs of primers, unique for each gene, i.e., *TLN1*, *NAMPT*, *MMP8*, *TAGLN2*, *PXN*, and *ITGAM*, are presented in Table S2. The ddPCR assays and data analysis were performed as described previously.[16] The level of each gene was calculated as the ratio of the absolute transcript level of genes to the geometric mean of the absolute transcript level of reference genes, *PGK1* and *GAPDH*.

2.5. Immunoassay Analysis

Ten patients' samples from each experimental group were chosen for immunoanalysis. The protein concentration was measured using a commercially available ELISA kit (Elabscience, China). ELISA validation was prepared for integrin beta-2 (ITGB2), integrin alpha-M (ITGAM), talin-1 (TLN1), and vinculin (VCL), identified in LC-MS/MS analysis. The concentrations of three known plasma integrin ligands, vascular cell adhesion protein 1 (VCAM1), intercellular adhesion molecule 1 (ICAM1), and E-selectin, were also measured. All assays were prepared according to the manufacturers' instructions, including appropriate positive and negative controls.

For Western blot (WB) validation, equal amounts of proteins (30 μg) were separated by SDS-PAGE (4−15%; Biorad, Hercules, USA). Due to the high molecular weight of TLN1 (270 kDa; ∼2540 amino acids), the electrophoretic runs were extended beyond the point that dye reached the bottom of the gel, allowing for better separation of proteins in this molecular range. The proteins were transferred overnight to a PVDF membrane. Blots were blocked with TBST containing 4% BSA and incubated overnight with the anti-TLN1 primary antibodies. Chemiluminescent detection was performed using the ChemiDoc XRS imaging system.

2.6. Validation of Results with Quantitative Multiple Reaction Monitoring

Twenty-five patients' samples from each experimental group were chosen for MRM validation. A list of peptides and transitions for VCAM1, ICAM1, ANXA2, and EGLN was created by the open software Skyline 20.1.0.31.[17] Two unique peptides and two transitions with rank 1 or 2 for each peptide were chosen. Two isotope-labeled peptides were spiked into samples and used as an internal standard. An overview of MRM analysis is presented in Table S3. Proteins were in-solution digested with trypsin, as described previously.[11] LC-MS/MS analysis was conducted using the UFLC system coupled to an ESI triple-quadrupole mass spectrometer (LC-MS-8060, Shimadzu, Kyoto, Japan). The separation of samples was achieved on an Acquity UPLC Peptide CSH C18 column, 1.7 μm i.d., particle size of 2 μm and pore size of 130 Å (150 × 1.0 mm; Waters, Milford, USA). The LC conditions were optimized as follows: solvent A was 0.1% formic acid in the water, and solvent B was 0.1% formic acid in acetonitrile. The gradient program for pump B was set as follows: 0.01−20 min, 10−65%; 20−25 min, 95%; and 25−30 min, 10%. The flow rate was set to 0.1 mL min^{-1}, and the column temperature was set at 40 °C. LabSolutions software (Shimadzu, Kyoto, Japan) was used to control the instruments as well as to acquire and process the data. Skyline software was used for MRM peak integration, normalization, and relative abundance calculations.

2.7. Statistical Analysis

Statistical analyses were performed using Perseus 1.6.1.3, Statistica 12.0 software (StatSoft, Inc., Kraków, Poland), or R ver. 3.6.0 and R Studio ver. 1.2.1335. All plots were made in R Studio, and the following packages were used: dplyr, ggplot2, reshape2, ggsignif, and ggpubr. Chi-square test was used for categorical variables. Data distribution was assessed using a Shapiro−Wilk test and Leven's test to evaluate the equality of variances. The data were statistically analyzed using a Mann−Whitney U-test or Student's unpaired *t*-test when appropriate. More than two groups were compared using one-way ANOVA or Kruskal−Wallis for non-parametric data, followed by post hoc multiple comparison testing. Statistical significance was accepted as $p < 0.05$. The Benjamini−Hochberg FDR was set to 5%.

Statistical power was calculated based on the number of biological replicates, FDR adjusted p-value and coefficients of variation calculated for all proteins. Because overall variation was below 30% for each experimental group, fold change 1.4 was chosen according to ref 18. Additionally, the effect size (Hedges's g) was calculated according to Cohen's d[19] formula corrected by Hedges's.[20] All differential proteins with Hedges's g below 0.5 were excluded from the final list of differential proteins. Therefore, a protein was considered to be differentially expressed if the difference between at least two groups was statistically significant ($p < 0.05$), the effect size was above 0.5, and the fold change was above 1.4. Only DEPs identified

https://doi.org/10.1021/acs.jproteome.0c00883
J. Proteome Res. 2021, 20, 3053−3067

with a minimum of two unique peptides, at >99% confidence level were accepted.

The correlations between variables were defined by the Pearson coefficients, and p-values less than 0.05 were considered significant. Multivariate analyses were carried out by unsupervised principal component analysis (PCA) and hierarchical clustering. For hierarchical clustering and heat map visualization, data were normalized to z-score.

2.8. Bioinformatic Analysis

Bioinformatic analysis was conducted using Perseus and Ingenuity Pathway Analysis software (Ingenuity Systems, Redwood City, USA). All identified proteins were annotated according to their Gene Ontology in the cellular compartment, canonical pathway, and biological function category using UniProtKB list. Differentially expressed proteins (DEPs; (p-value <0.05; fold change ≥1.4; effect size >0.5; ≥2 unique peptides) were subjected to the enrichment analysis to determine the top cellular compartment, canonical pathways, biological functions, and upstream regulators associated with the observed differences in protein profiles. Also, downstream effect analyses were performed from which the most affected categories were extracted. Enrichment analysis was performed using the right-tailed Fisher's exact test with Benjamini–Hochberg (B-H) multiple corrections. Based on obtained p-value, this test estimates the probability that the association between a set of molecules and a function or pathway is not random. Moreover, the IPA regulation z-score algorithm was also used to predict the direction of change for a given function or pathway. A negative z-score indicates inhibition, and positive predicts activation. In order to enhance the stringency of our analysis, functions with z-scores ≥2 (for activation) and ≤−2 (for inhibition) were considered as those in which the directionality was assigned.[21] The z-score was not calculated if there were no available data in the Ingenuity Knowledge Base concerning the functional involvement of the given DEPs. In case the directionalities of changes in the data set and those predicted by the Ingenuity Knowledge Base were not corresponding, a "biased" z-score was defined.

2.9. Data Availability

The mass spectrometry proteomics data have been deposited to the PRIDE Archive (http://www.ebi.ac.uk/pride/archive/) via the PRIDE partner repository with the data set identifier PXD018596 (https://www.ebi.ac.uk/pride/archive/projects/PXD018596).

3. RESULTS

The whole leukocyte fraction of peripheral blood was collected from two experimental groups with CKD (CKD1-2 and CKD5), two groups with CVD (CVD1 and CVD2), and healthy volunteers (HVs). Based on similar symptoms and results of medical examinations, the equal status of atherosclerosis progression was concluded for CKD1-2/CVD1 groups as well as for CKD5/CVD2 groups. A characteristic of each analyzed group is presented in Table 1. Samples did not differ in their white blood cells number. Also, the number of granulocytes and lymphocytes, which constitute approximately 90% of all leukocyte population, did not reveal statistical differences (according to Mann–Whitney U-test) between CVD or CKD patients groups. Only the number of monocytes was elevated in CKD5 compared to other groups (Table 1). Fluorescence microscopy and flow cytometry were utilized to evaluate the quality of collected samples and the percentage of leukocyte subpopulations (Figure S1). The obtained results confirmed the data derived from medical examinations and revealed an increased number of monocytes in CKD5 samples (average 9.6% ± 1.06) as compared to other patient groups (average 6.5% ± 0.39) ($p < 0.01$). Therefore, correlation analyses between the identified proteins and the number of particular blood cells and leukocyte subpopulations were performed, in order to exclude the probable influence of this observation on obtained proteomic results (see results for DEPs below and in Table S4).

Isolated cells were lysed, and proteins were analyzed by nano-LC-MS/MS, which resulted in the identification and quantitation of 2845 proteins in total. Enrichment analysis using Fisher's exact test determined the presence of 2320 proteins with intracellular localization (B-H-corrected p-value 6.68×10^{-268}), and 525 extracellular proteins. Since the analyzed experimental groups slightly differed in the context of statin and anticoagulant treatment (Table 1), we also statistically evaluated if proteins with differential abundances were related to the applied therapy. Then the data were filtered, and only proteins detected in all samples (1687) were taken into account in the quantitative analyses. A total of 149 differentially expressed proteins (DEPs), whose abundance was significantly altered amid analyzed groups (Table S5), were included in the subsequent bioinformatic surveys. Enrichment analysis in the context of compartmental localization was performed for DEPs, and the results were compared with those obtained for all proteins identified in the study. According to the value of enrichment factor and B-H-corrected FDR p-value, the distribution of all categories was similar in both sets of proteins (Figure S2).

PCA revealed that CKD5 and CVD2 differed most significantly between each other and separated from the other groups (Figure S3). The obtained quantitative data confirmed this result—118 proteins out of 149 revealed significant differences only when the CKD5 and CVD2 groups were compared. Among 118 proteins differentiating CKD5 and CVD2 groups, 107 of them showed a "large" effect size with a value above 0.8. Moreover, the average effect size for this set of DEPs was 1.24, suggesting their significant influence on differentiating both groups. These DEPs were further queried by hierarchical clustering. In the CVD2 group, an abundance of 53 proteins was decreased as compared to CKD5, while 65 proteins were downregulated in CKD5 in comparison to CVD2 (Figure S4). Several of these proteins differentiated also CKD5 from other experimental groups (Table S5).

To reveal possible relationships, in the next step, 118 DEPs were correlated using the Pearson correlation, and the resulting matrix was visualized as a heat map (Figure S5). More details about these correlations are presented in other parts of the study (Table S6).

Correlation analyses were also performed between DEPs and the number of particular cells subpopulations and results from medical examinations. No correlated DEPs were identified. Even the number of monocytes revealed Pearson coefficients below 0.3 and above −0.3. Thus, there were no DEPs correlating with the number of monocytes. However, monocytes negatively correlated with eGFR ($r = -0.63$), suggesting a putative relationship with CKD progression (Table S4).

The abundance of eight proteins (ITGAM, ITGB2, PXN, TLN1, VCL, MMP8, NAMPT, and ANXA2) was validated using an ELISA, WB, MRM, or ddPCR approach. The

https://doi.org/10.1021/acs.jproteome.0c00883
J. Proteome Res. 2021, 20, 3053−3067

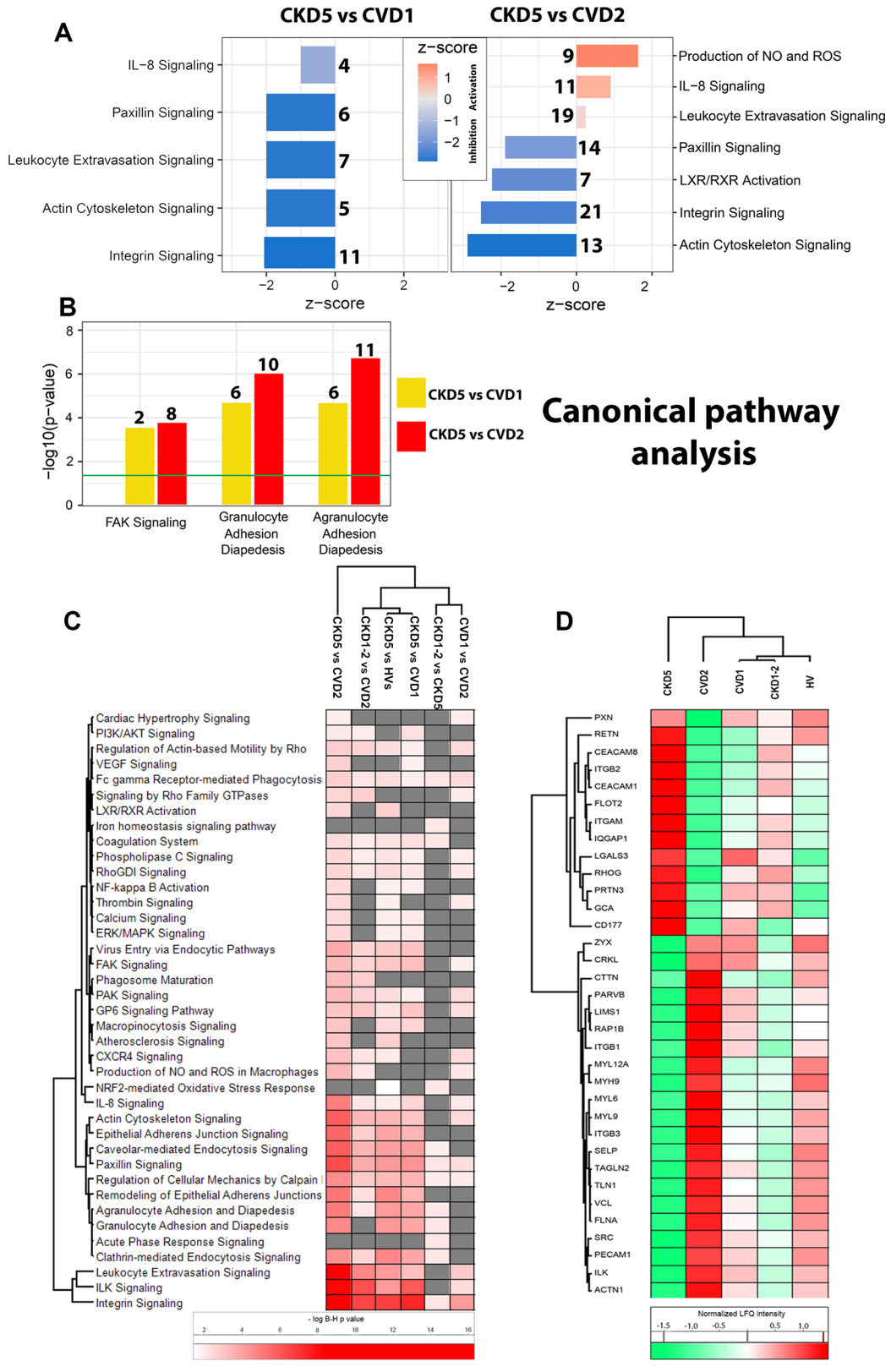

Figure 1. Canonical pathway analysis. (A) The chart of the top statistically enriched pathways according to Ingenuity Pathway Analysis (IPA) calculations presents *z*-scores and the number of DEPs (bold) associated with each pathway. Comparisons CKD5 vs CVD1 and CVD2 are presented. Inhibited in CKD5 pathways are marked in blue. Pathways activated in CKD5 are depicted in red. (B) Top canonical pathways without predicted *z*-scores but significantly enriched according to IPA derived Fisher's test. A threshold of $-\log_{10}$ B-H-corrected *p*-value 1.3 (green line) represents a *p*-value 0.05. Numbers indicate the number of DEPs associated with each pathway. (C) The heat map presents the top statistically enriched pathways in all comparisons. Functions that were not enriched in a particular comparison are presented in gray. (D) The heat map presents abundances of DEPs involved in actin cytoskeleton, integrin signaling, and leukocyte extravasation—the most statistically enriched pathways in the study. A detailed list of annotations is presented in Table S7.

https://doi.org/10.1021/acs.jproteome.0c00883
J. Proteome Res. 2021, 20, 3053−3067

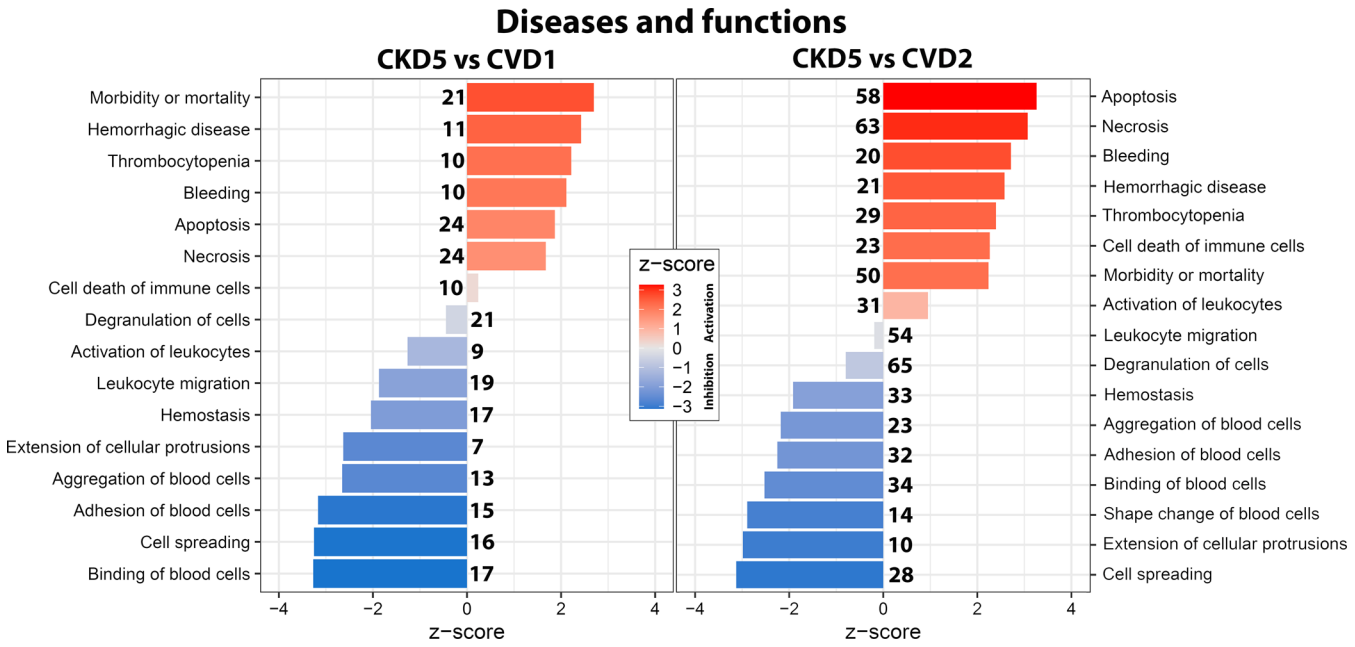

Figure 2. Functional analyses of DEPs identified in CKD5 vs CVD1/CVD2 comparisons. The chart of the top statistically enriched functional categories according to IPA calculations presents *z*-scores and the number of identified DEPs (numbers in bold) associated with each category. Inhibited categories in CKD5 are marked in blue. Functions activated in CKD5 are marked in red. A detailed list of annotations is presented in Table S7.

abundance of TLN1 was confirmed utilizing two different methods, MRM and WB.

3.1. Integrin and Actin Cytoskeleton Signaling Pathways Are Highlighted in CKD vs CVD Comparison

To assign the functional relationships, the DEPs were queried utilizing Ingenuity canonical pathways classification (Figure 1A,B). Six comparisons between experimental groups with the highest number of identified DEPs were chosen for IPA analysis (Figure 1C). Overall, 37 different canonical pathways were overrepresented according to B-H *p*-value (Table S7) and statistically enriched in CKD5 versus CVD2 comparison. The top-ranked canonical pathways included integrin signaling and leukocyte extravasation signaling as well as ILK, paxillin, and actin cytoskeleton signaling (Figure 1A−C).

We also analyzed the directionality of the overrepresented canonical pathways. For this purpose, we used the IPA *z*-score algorithm to identify pathway categories that are expected to be activated (positive *z*-score) or inhibited (negative *z*-score) between analyzed experimental groups. We revealed that actin cytoskeleton, integrin, and paxillin signaling pathways were the most inhibited in CKD5 compared to CVD2 and CVD1 (Figure 1A). On the other hand, the leukocyte extravasation signaling pathway, sharing many proteins with integrin and actin signaling pathways and being the second most overrepresented pathway, did not reveal any significant directionality (*z*-score ∼0) (Figure 1A). We thus decided to more closely examine the abundance of 34 DEPs assigned by IPA analyses to the actin cytoskeleton, integrin signaling, and leukocyte extravasation categories. By comparing the abundance of these proteins, we found that 13 of the 34 DEPs were upregulated in CKD5 (Figure 1D). Some of these proteins were also increased in the CKD1-2 group (9 out of 34).

3.2. Leukocyte Migration and Diapedesis-Related Proteins Are Dysregulated in CKD vs CVD

To gain more functional insight, we further analyzed DEPs in the context of associated functions and diseases (Figure 2). This analysis confirmed the results obtained in the canonical pathway study and revealed overrepresented categories associated with leukocyte activation and migration. Some of them (cell spreading, shape change of blood cells, binding, adhesion, and aggregation of blood cells) were predicted to be inhibited in CKD5 when compared to CVD2 and CVD1. However, overrepresented functions related to cell movement and degranulation did not disclose any significant directionality as suggested by their *z*-scores.

To confirm the validity of our findings, the differential abundance of selected proteins involved in integrin and actin cytoskeletons signaling during the leukocyte diapedesis process (ITGAM, ITGB2, PXN, TLN1, and VCL) was further assessed. It was evaluated by ELISA (ITGB2, ITGAM, and VCL), MRM (ANXA2), and WB (TLN1), and at the mRNA level by ddPCR (*ITGAM*, *PXN*, and *TLN1*). Validation at the protein level partially confirmed proteomic findings and bioinformatic predictions. The expression of *PXN* and *ITGAM* was not altered at the mRNA level, suggesting that differential changes may be related to posttranslational events (Figure 3A). Since integrins can bind to a number of adhesion molecules produced by endothelial cells and released to plasma, we subsequently scrutinized an abundance of well-characterized plasma integrin ligands: VCAM1, ICAM1, and E-selectin (Figure 3B). Level of expression of these plasma adhesion molecules was significantly elevated in CKD5 as compared to CVD2 and HVs, which was confirmed by two independent methods, MRM and ELISA. Previously, it has been demonstrated that endoglin (EGLN) inhibits the synthesis of several members of the integrin family and regulates integrin-mediated cell adhesion (reviewed in ref 22), and we thus decided to check the level of this protein in

https://doi.org/10.1021/acs.jproteome.0c00883
J. Proteome Res. 2021, 20, 3053−3067

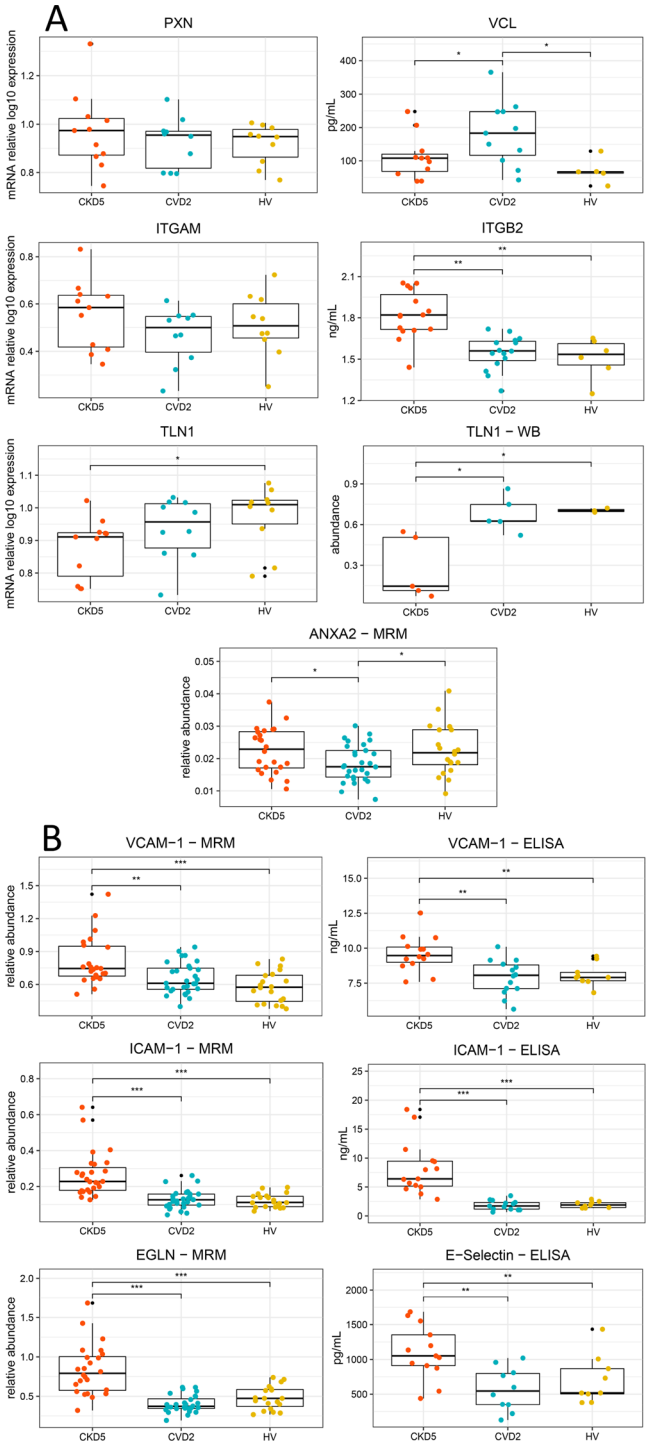

Figure 3. (A) Validation using ddPCR (*PXN*, *ITGAM*, *TLN1*), ELISA (ITGB2, VCL), MRM (ANXA2), and WB (TLN1) methods. Boxes on plots represent interquartile ranges and median. (B) Quantitative ELISA and MRM measurements of selected proteins involved in the integrin signaling pathway, synthesized by endothelium and secreted to plasma. Mann−Whitney U-test. $*p < 0.05$, $**p < 0.01$, $***p < 0.001$; $n = 10$ (ELISA), $n = 25$ (MRM), $n = 5$ (WB) in each group.

plasma. The abundance of the soluble form of endoglin was twice higher in CKD5 in comparison to CVD2 and HVs (Figure 3B).

Taken together, utilizing different targeted and non-targeted proteomic approaches, we detected 17 upregulated and 21 downregulated proteins in CKD5 that were functionally related to the actin cytoskeleton, integrin cascade, and leukocyte migration signaling. These experimental results are graphically illustrated in Figure 4. The majority of proteins involved in the initial steps of leukocyte capture from the bloodstream and rolling on the luminal surface of endothelial cells were differentially upregulated (depicted in red color). Increased expression was also detected for ligands and their receptors expressed on endothelium and leukocytes, i.e., E-selectin (SELE), ICAM1, VCAM1, and ICAM3, as well as for some associated proteins, involved in leukocyte adhesion. Both components of integrin MAC1/$\alpha M\beta 2$ (ITGB2 and ITGAM), specifically expressed by neutrophils and monocytes, were upregulated in CKD5. Among this group of proteins, only P-selectin (SELP) was downregulated. The binding of leukocytes' integrins to their extracellular ligands triggers signaling cascades designated as "outside-in signaling", which leads to the strengthening of leukocyte adhesion and their movement. We found that most DEPs participating in the later phase of transmigration, apart from paxillin, were down-regulated (marked in green in Figure 4). The expression of actin-binding proteins, i.e., VCL, TLN1, ZYX, and proteins regulating the reorganization and polarization of actin cytoskeleton during movement and diapedesis, was decreased. Therefore, the observed changes may partially explain the lack of specified directionality (suggested by biased-z-score) for integrin and actin cytoskeleton signaling and diapedesis-related categories. Correlation analysis revealed that many proteins belonging to both groups of proteins (depicted in Figure 4, in red and green) were associated with each other, i.e., ITGAM negatively correlated with TLN1 ($r = -0.74$), TAGLN2 ($r = -0.73$), FLNA ($r = -0.72$), or VCL ($r = -0.69$). On the other hand, proteins found to be in the same functional group displayed very strong and positive relationships; i.e., ITGB2 correlated with ITGAM ($r = 0.86$), and TLN1 as revealed by Pearson correlation coefficients above 0.9 for VCL, FLNA, or TAGLN1 (0.95, 0.97, and 0.93, respectively; Table S6).

3.3. Advanced CKD Group Discloses a Higher Rate of Apoptosis

Moreover, the obtained results revealed dysregulation of processes related to cell death and survival. The necrosis and apoptosis pathways were activated in the CKD5 as compared to CVD2 (z-scores of 3.07 and 3.26, respectively, Figure 2) and CKD1-2 (z-scores of 1.96 and 2.88, Table S7). Activation of these processes was also predicted in CKD5 group versus CVD1 comparison, albeit with a less pronounced effect (z-scores of 1.67 and 1.86, respectively). Similarly, morbidity/mortality and cell death of immune cells were identified as activated in CKD5 compared to CVD2 (z-scores of 2.69 and 2.64, respectively) and CVD1 (z-scores of 2.23 and 0.23, respectively).

Flow cytometric analysis of necrosis and apoptosis rate in examined cells, performed by staining with CellEvent Casp3/7 in conjunction with propidium iodide, confirmed these predictions (Figure 5A). The percentage of live cells in CVD2 samples was calculated at 95.74% ± 2.95, whereas CKD5 samples demonstrated on average 76% ± 6.38 of live cells, and these differences were statistically significant ($p < 0.001$), (Figure 5B). Specifically, the number of late apoptotic cells was highly increased in CKD5 compared to CVD2 (14% ±2 as compared to 3.7% ± 0.7; $p < 0.001$). More than 20 DEPs related to cell death and survival were identified, all of

https://doi.org/10.1021/acs.jproteome.0c00883
J. Proteome Res. 2021, 20, 3053−3067

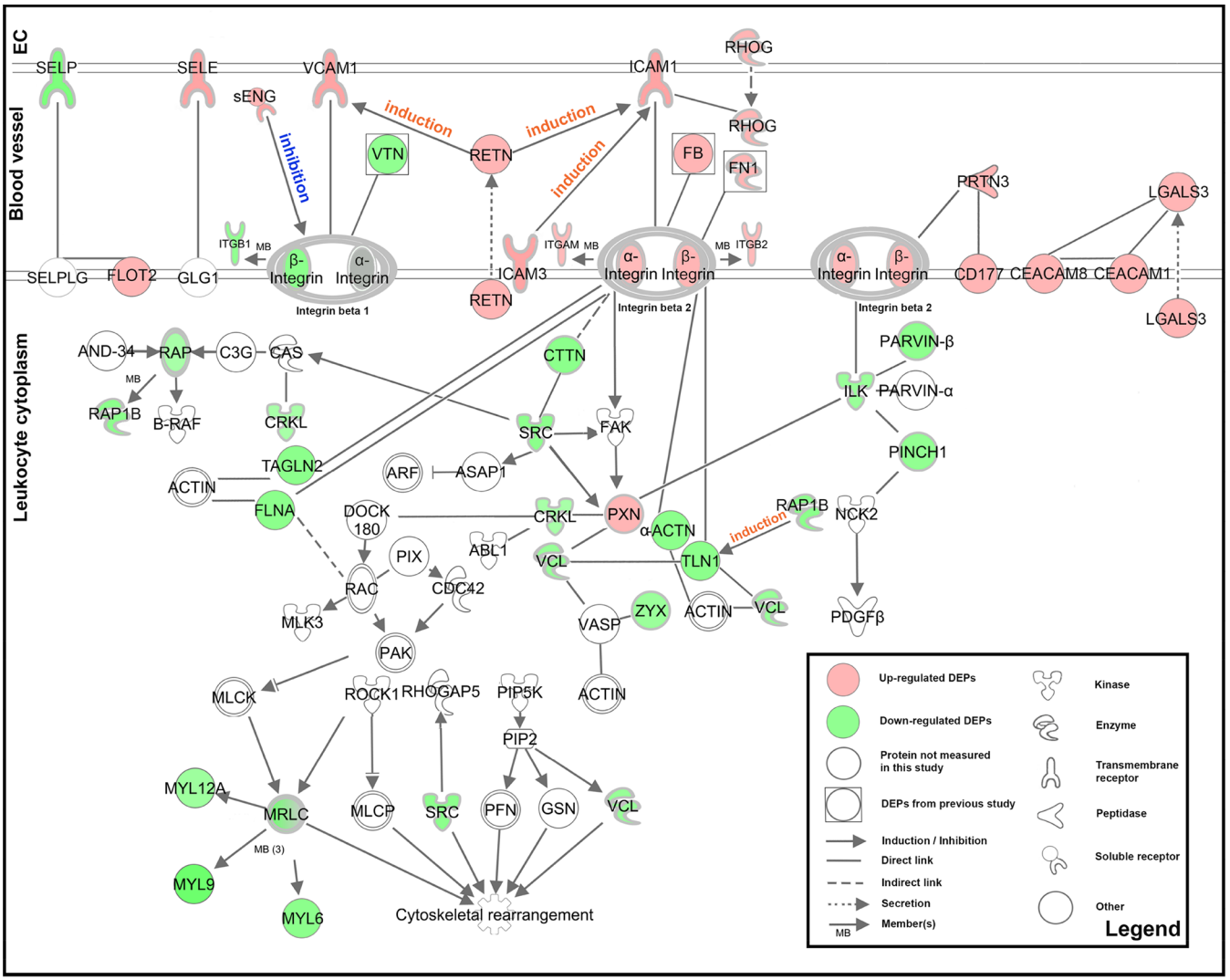

Figure 4. Pathway illustrating the involvement of DEPs identified in CKD5 vs CVD2 comparison in integrin/actin signaling processes during leukocyte extravasation. An increase in CKD5 expression (depicted in red) was detected for ligands and their receptors expressed on both endothelium and leukocyte surface, as well as for proteins regulating activation and adhesion. Downregulation observed in CKD5 (depicted in green) was characteristic for actin-binding proteins and proteins regulating the reorganization and polarization of actin cytoskeleton during diapedesis. Three DEPs identified in the previous study, namely vitronectin (VTN), fibrinogen (FB), and fibronectin 1 (FN1) (depicted by squares),[11] and corroborated by the currents findings, were added as components of the pathways.

them found to be upregulated in CKD5. Majority of these proteins positively correlated with each other (Table S6). Moreover, a Pearson's correlation test revealed that many of these proteins were negatively correlated with eGFR, i.e., NCF1, NCF2, NAMPT, MMP8, MMP9, ANXA1, ANXA3, and ANXA11 (all with $r < -0.5$). It suggests that upregulation of necrosis and apoptosis processes is closely associated with the progression of renal dysfunction. To validate this finding, two proteins categorized by IPA software as participated in apoptosis, NAMPT and MMP8, were validated by ddPCR method at the mRNA level (Figure 5C). Correlation analysis between particular DEPs revealed that many identified proteins involved in apoptotic processes displayed a positive relationship with a group of upregulated proteins engaged in cell adhesion and migration. For instance, ITGAM and ITGB2 correlated with MMP9, NCF1, NCF2, ANXA1, and ANXA3 with average correlation coefficients of 0.77 and 0.61, respectively. Similarly, the same apoptotic proteins were found to be negatively correlated with many downregulated in CKD5 diapedesis proteins (see details in Table S6). This observation suggests that alterations in the abundance of proteins related to integrin and actin cytoskeleton pathways, and cell adhesion and movement, can be closely associated with an elevated rate of apoptosis and mortality in CKD5 cells observed in proteomics and microscopy/flow cytometry analyses.

Apart from cell death and survival, the functions linked to hemostasis, i.e., thrombocytopenia and hemorrhagic disease (19 and 21 DEPs, respectively), were activated in CKD5 as compared to CVD2 (z-scores 2.39 and 2.57), and to a lesser extent versus CVD1 (z-scores 2.21 and 2.42, Figure 2) and CKD1-2 (z-scores 2 for both, Table S7).

Irrespective of cardiovascular background, we also tried to reveal how the progression of CKD influences the composition of leukocytes' proteome. For this purpose, we compared both groups of CKD and HVs. Functional analysis revealed categories enriched specifically in CKD1-2 as compared to CKD5. For instance, the flux of ions (z-score 2.17), ion

https://doi.org/10.1021/acs.jproteome.0c00883
J. Proteome Res. 2021, 20, 3053−3067

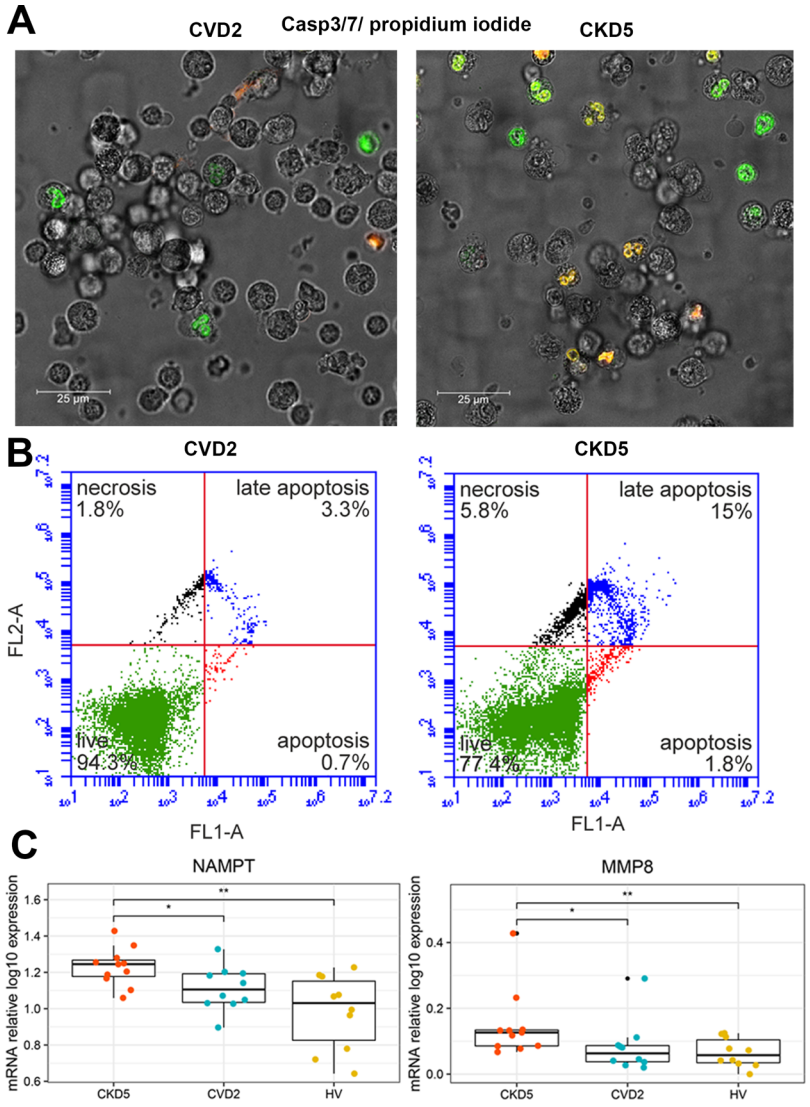

Figure 5. Upregulation of apoptosis in CKD5. Dysregulation of processes related to cell death revealed by bioinformatic analysis confirmed by (A) confocal microscopy (green, apoptotic cells; orange, dead cells) and (B) flow cytometric analysis assessing apoptosis/necrosis in representative CVD2 and CKD5 samples. (C) Validation of *NAMPT* and *MMP8* at the transcriptome level using ddPCR, corroborated the results of proteome profiling using nano-LC-MS/MS. Mann−Whitney U: $*p < 0.05$, $**p < 0.01$; $n = 10$ in each group.

homeostasis of cells (*z*-score 2.23), cell viability (*z*-score 2.71), cellular infiltration by leukocytes (*z*-score 2.21), and homing of cells (*z*-score 2.39) were more pronounced at the initial stage of CKD (Table S7 and Figure S6). Comparing both CKD groups also revealed categories related to the blood coagulation cascade and hemostasis, and suggested that these processes are more perturbed at the advanced stage of CKD. Also, functions related to apoptosis and necrosis were clearly upregulated in CKD5 compared to CKD1-2. However, these differences were not as pronounced when comparing CKD5 to CVD2 (Table S7).

Many functional categories were statistically enriched also in CVD1 as compared to CVD2. Stimulation of cells, the immune response of leukocytes, migration of leukocytes, atherosclerosis, and occlusion of arteries were predicted to be activated in CVD1 in comparison to CVD2, with *z*-scores close to 2 (1.95−1.98). On the other hand, several "general inflammation" categories, like organ inflammation (*z*-score 1.87), were upregulated in CVD2 group as compared to CVD1.

Finally, we analyzed a proteomic profile of healthy volunteers in comparison to particular patients' groups. Not surprisingly, the highest differences were revealed in HVs vs CKD5 comparison. Although enriched canonical pathway and function categories were similar to those indicated in the comparison between CKD5 and other groups of patients, the intensity of observed differences was very often higher based on *z*-score values. For example, *z*-score for hemostasis function was revealed as 2.0 for CKD1-2 vs CKD5 comparison, whereas for HVs vs CKD5 this value was more significant and amounted to 2.7 (Table S7).

3.4. TGFB1, SRF, and GATA1 Are the Primary Upstream Regulators at the Protein Level

To identify the regulators predicted to be activated or suppressed in the cascade, the DEPs were functionally linked to upstream network drivers. Transforming Growth Factor Beta 1 (TGFB1) was identified as a top upstream regulator in all comparisons, according to B-H-corrected *p*-value. However, according to a *z*-score (−1.70 and −1.73 for CKD5 vs CVD2 and CKD5 vs CVD1 comparisons, respectively) directionality

https://doi.org/10.1021/acs.jproteome.0c00883
J. Proteome Res. 2021, 20, 3053−3067

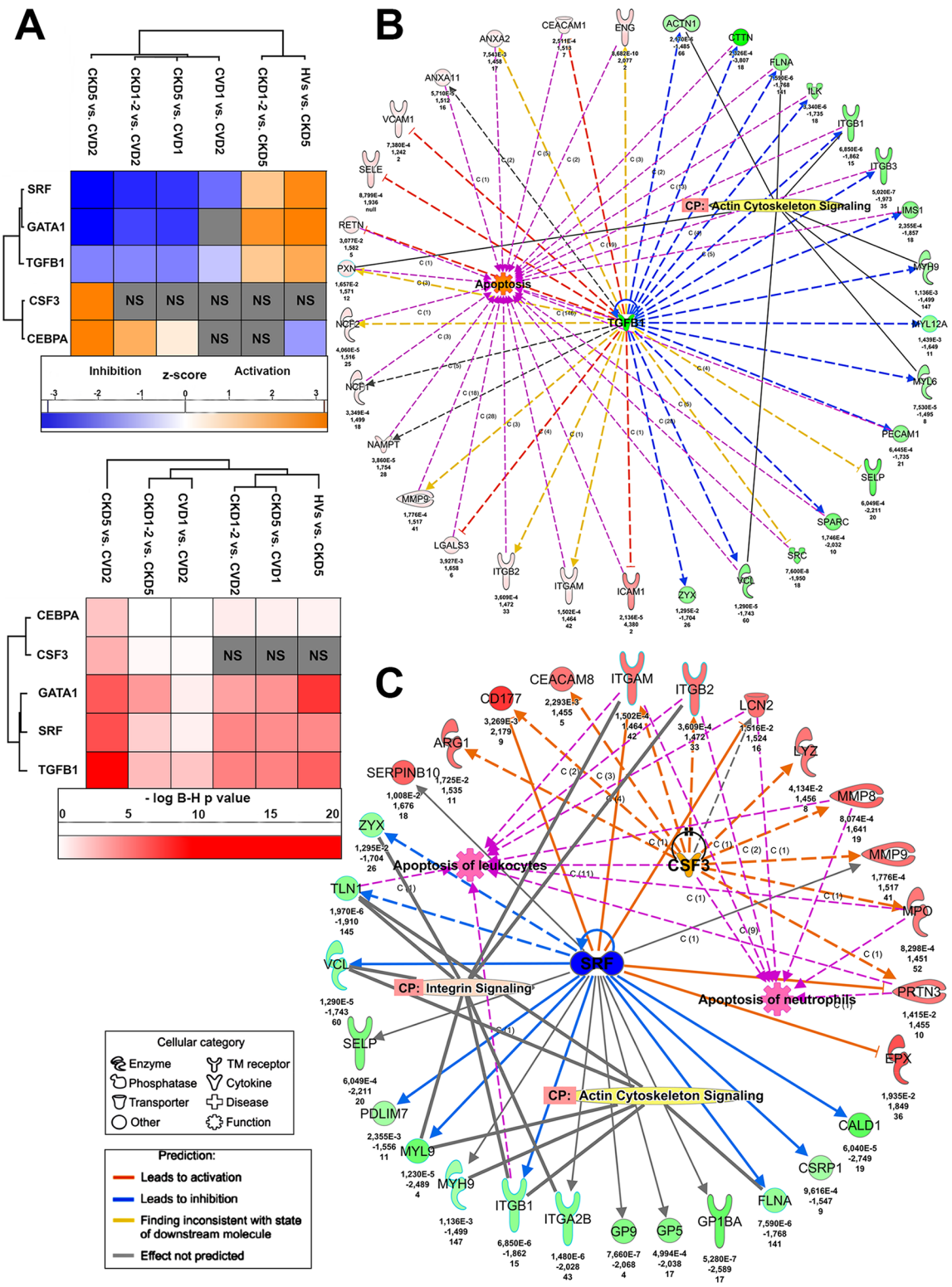

Figure 6. Upstream regulators analysis using Ingenuity Pathway Analysis software. (A) The top upstream regulators with predicted activation/inhibition state according to calculated *z*-score (the upper heat map) and B-H-corrected *p*-value (the lower heat map). Functions overrepresented according to B-H-corrected *p*-value but without calculated *z*-scores are present in gray. Functions not enriched according to B-H-corrected *p*-value are present in gray with NS. A detailed list of annotations is presented in the Table S7. (B) The network displays predicted interactions between DEPs identified in CKD5 vs CVD2 comparison and the top upstream regulator according to B-H-corrected *p*-value: TGFB1. Links with apoptosis and actin cytoskeleton categories are presented. (C) The network displays predicted interactions between DEPs identified in CKD5 vs CVD2 comparison and the top upstream regulators, according to *z*-score: SRF and CSF3. Links with apoptosis and integrin signaling categories are presented. The downregulated in CKD5 compared to CVD2 proteins are shown in green and upregulated ones in red. The arrows indicate the directionality of changes. Solid and dashed lines indicate experimentally confirmed and predicted interactions, respectively. Numbers by the nodes in panels B and C refer to B-H-corrected *p*-values, fold changes, and the number of unique peptides, respectively.

https://doi.org/10.1021/acs.jproteome.0c00883
J. Proteome Res. 2021, 20, 3053−3067

was not predicted, suggesting crosstalk with other cellular processes which may influence the score (Figure 6A and Table S7). To functionally bridge these findings, we further connected 33 DEPs predicted to be regulated by TGFB1 (Figure 6B). The network analysis revealed that TGFB1 is an upstream regulator of a cell migration process, including actin cytoskeleton organization and signaling (dysregulated in CKD5), and regulates apoptotic/necrotic processes (upregulated in CKD5). This result is consistent with the dysregulation of canonical pathways and biological functions observed in CVD and CKD. The top upstream regulators with predicted inhibition included transcription factors: serum response factor (SRF) and GATA-binding factor 1 (GATA1) (Figure 6A, Table S7). Twenty-two DEPs were predicted to be regulated by SRF, and 15 of them were downregulated in CKD5 in comparison to CVD2 (Figure 6C). Colony stimulating factor 3 (CSF3) and CCAAT enhancer binding protein alpha (CEBPA) were predicted to be the top positive regulators of the networks, uniquely in CKD5 versus CVD2 comparison. Eleven DEPs involved in cell death/survival categories and processes related to inflammation were predicted to be downstream targets for CSF3 and upregulated in their expression in CKD5 versus CVD2 comparison (Figure 6C). Moreover, other proteins predicted to be upregulated due to reduced expression level of SRF, constituted a part of these functional categories. The proteins negatively regulated by SRF belong to cell−cell aggregation, adhesion, and transmigration processes and integrin, paxillin, and actin cytoskeleton signaling pathways. Although, the relationship between SRF and atherosclerosis in classical CVD patients is not novel, the underlying alterations observed in CKD and the differences between CKD and CVD have not yet been presented.

4. DISCUSSION

Although CKD is a disorder associated with a loss of renal function, these patients are exposed to a high risk of atherosclerosis. The predominant causes of their deaths are cardiovascular events.[23,24] Atherosclerosis is an inflammatory disease, and during its progression, various types of immune cells play essential roles in the initiation and progression of atherosclerotic plaques. During the progression of atherosclerosis unrelated to kidney dysfunction, monocytes are recruited to the intima and, due to dyslipidemia, differentiate into foam cells, which triggers atherosclerotic plaque formation.[25] The accumulation of inflammatory cells and lipids in the arteries leads to the formation of mature plaques and the thickening of their walls. In contrast, due to "reverse epidemiology", CKD patients do not reveal typical dyslipidemia, and their plaques show more inorganic character.[26] Nonetheless, systemic inflammation is undoubtedly elevated in CKD (reviewed in ref 27).

Our previous studies utilizing patients' plasma samples indicated an upregulation of systemic inflammation during CKD development and confirmed that this phenomenon is more pronounced in CKD compared to the "classical" CVD.[11] At present, in order to provide deeper insights into the inflammation-based mechanisms underlying atherosclerosis-related and non-related to CKD, we utilized the proteomic approach to investigate the global protein profiles of the immune system cells, focusing on leukocytes isolated from the patients at the initial and advanced stages of CKD and CVD. We also subsequently scrutinized the abundance of molecules produced by endothelial cells and released to plasma to link the literature findings with proteomic results. Correlation analysis revealed that there is no association between identified DEPs and the particular leukocyte subpopulations. The number of monocytes, which differentiated CKD5 from the other groups, did not show any correlation with DEPs. However, considering that monocytes compose below 10% of all leukocytes, this result is not surprising. Nevertheless, we demonstrated that monocytes negatively correlated with CKD progression what was presented before,[28] but never revealed in the currently presented experimental setup.

Our results show that CKD5 and CVD2 groups, representing patients with similar advanced symptoms of CVD but differing in renal function, reveal the most differences in proteomic profiles. The CKD1-2 and CVD1 groups, which signify patients with initial atherosclerosis symptoms, showed a high level of similarity in their protein profiles. These results are consistent with those presented in our previous study utilizing plasma samples.[11,29] In the present study, we demonstrated for the first time that CKD leukocytes phenotypically differ from those derived from CVD patients, in the dynamics of their biological pathways and processes related to cell−cell adhesion and transmigration machinery (as judged by the differential expression of several pathway components). Several canonical pathways and processes related to leukocyte rolling and adhesion and the subsequent migration to the sites of inflammation were found dysregulated in comparison amid CKD5 and CVD2. In other comparisons, i.e., CKD5 vs CVD1 and CKD1-2 vs CVD2, these pathways were also found to be statistically differentially enriched, but with lesser significance. Notably, only early steps, but not initial, of leukocyte adhesion and rolling on the surface of endothelial cells were differentially upregulated in CKD compared to CVD (Figure 4). P-selectin is responsible for the initial stage of leukocyte arrest on endothelium, but its level of expression was decreased in CKD5. Importantly, maximal expression of this protein has been observed after 10 min of leukocyte activation, after which E-selectin and other proteins identified as upregulated in our study take over its role.[30]

Selectins interact with receptors present on the surface of leukocytes with marginal affinity, which results in a reduction of leukocytes velocity. The tight binding and arrest of leukocytes on endothelium are mediated by the interaction of integrins with their ligands, which leads to the strengthening of adhesion.[31] Several reports have demonstrated the increased level of ligands, i.e., VCAM1 and ICAM1 in CVD patients as the factor promoting atherosclerosis development,[32−34] to our knowledge, this is the first study directly comparing CKD and CVD patients in this context. The upregulation of integrins in CKD in comparison to CVD has not been demonstrated earlier. Crawling of the leukocytes to endothelial junctions is almost exclusively dependent on interactions between leukocyte-specific β2 integrins MAC1 and LFA-1 and their ligands, ICAM1 and ICAM3.[35,36] The increased expression level of ICAM1, ICAM3, and other molecules interacting with them and β2 integrins MAC1 and LFA-1 suggest the upregulation of MAC1/LFA4-ICAM-dependent crawling mechanism determining the subsequent stage of the leukocyte adhesion cascade. These integrins play vital roles in leukocyte targeting to the atherosclerotic plaques.[31] Their upregulation can affect the ability of leukocytes to adhere to the endothelium and promote the local accumulation of the leukocytes on endothelium, which supports pro-inflammatory conditions and atherosclerotic plaques' development.

https://doi.org/10.1021/acs.jproteome.0c00883
J. Proteome Res. 2021, 20, 3053−3067

Endoglin is another transmembrane molecule that interacts with β1-type integrin and promotes leukocytes' migration to the inflammatory site.[37] However, it has been presented that the soluble form of endoglin inhibits leukocyte extravasation.[38] We demonstrated an increased abundance of this specific form of endoglin. It may explain the decreased level of ITGB1, a component of β1 integrin VLA-4. Furthermore, the reduced expression level of vitronectin, one of the ligands for β1 integrin in CKD5 was previously demonstrated by us.[11]

In a physiological state, adhesion of leukocytes to endothelial cells leads to cell motility, by controlling cytoskeletal rearrangements causing transendothelial migration. Actin cytoskeleton assembly and its dynamics are pivotal for cell migration and immune response involving leukocytes. In our study, almost all DEPs participating in the later transmigration phase were downregulated in the CKD5 group (Figure 4). Among those were actin-binding proteins as well as proteins regulating the reorganization of the actin cytoskeleton. Paxillin acts as an adaptor stabilizing the linkage of VLA-4 to actin cytoskeleton during leukocyte adhesion upon exposure to fluid flow and transmission of mechanical force,[39] which partially can explain its increased expression level.

Leukocytes can sense and resist high external forces from flowing blood through RAP1 and PI3K regulation of actin polymerization.[40] In our analysis, downregulation of RAP1 and disturbances in expression of other proteins regulating the cytoskeleton among the CKD5 and CVD2 groups were identified. Rullo and co-workers[40] suggested that reinforcement of tension-bearing structures by actin is critical for adaptation of cells to the external force. Therefore, decreased ability of CKD5 cells to actin cytoskeleton reorganization during the transmigration process might be compensated by the mechanism of stabilization of leukocytes on the surface of endothelium by integrin-related mechanism(s). Both phenomena might influence endothelial dysfunction and acceleration of atherosclerosis progression.

Under these circumstances, the observed upregulation of processes related to apoptosis in CKD5 further confirmed by flow cytometry and confocal microscopy analysis is not surprising (Figure 5). The misbalance between different phases of leukocyte extravasation may lead to the alteration of cellular integrity and trigger cell death. We have not detected differences in the number of leukocytes. It has been shown, however, that even though neutrophils undergo apoptosis, they are still able to prolong their longevity and survive for many hours before disintegration.[41] Moreover, a direct relationship between apoptosis and loss of cytoskeletal functions has been demonstrated.[42] On the other hand, the increased apoptosis resulting from oxidative stress in CKD is known (reviewed by[43]). Uremia and circulating uremic toxins evoke an imbalance between antioxidant protection and reactive oxygen species production, resulting in endothelial dysfunction leading to advanced CKD. Our previous study described that oxidative stress is more pronounced in CKD-related atherosclerosis than in classical CVD.[11] We also suggested that due to the progression of kidney dysfunction, CVD acceleration can be different at the initial and advanced stages of CKD, which might partially explain the differences between CKD5 and CVD2 profiles. In this study, we added another piece of the puzzle to the story: dysregulation in leukocytes' adhesion and extravasation processes.

However, apart from associations between CKD and CVD, we also confirmed that the progression of CKD and CVD itself influences on the composition of leukocytes' proteome. We have shown an upregulation of proteins related to inflammatory processes in advanced CVD. We have also indicated an ionic homeostasis and blood coagulation cascade, specifically associated with CKD progression.

Limitations inherent in this study should also be taken into account. Although this study sheds some light on the mechanism of chronic kidney disease-related atherosclerosis, the clinical significance and statistical power would undoubtedly benefit from more numerous cohorts. Nevertheless, our results underline the importance and necessity of studying and comparing patients with CKD and CVD in one study, and constitute a promising prelude for future work.

5. CONCLUSIONS

In the present study, we utilized proteomic profiling of leukocytes and demonstrated for the first time a dysregulation of proteins involved in different phases of leukocytes' transmigration which are very pronounced at the advanced stage of CKD. Moreover, the upregulation of proteins related to apoptotic cell death was also observed, which was functionally confirmed on the cellular level. The observed misbalance can lead to inflammation and, as a consequence, endothelial dysfunction and atherosclerotic plaque development.

■ ASSOCIATED CONTENT

Supporting Information

The Supporting Information is available free of charge at https://pubs.acs.org/doi/10.1021/acs.jproteome.0c00883.

Figure S1, microscopy and flow cytometry analysis of isolated cells; Figure S2, enrichment analysis in the context of compartmental localization; Figure S3, unsupervised principal component analysis; Figure S4, heat maps presenting abundance of identified DEPs; Figure S5, correlation coefficient matrix for DEPs in CKD5 vs CVD2 comparison; Figure S6, IPA functional analysis; Figure S7, TLN1 immunoblots for entire membranes (PDF)

Table S1, Pearson's correlation coefficients between the label-free quantification intensities from replicates in all experimental groups (XLSX)

Table S2, list of primers used in ddPCR analysis (XLSX)

Table S3, list of peptide transitions with precursor and product masses, charges, retention times, and collision energies used for MRM analysis (XLSX)

Table S4, results of correlation analyses between the identified DEPs and eGFR, including the number of particular blood cells and leukocyte subpopulations (XLSX)

Table S5, complete list of DEPs identified in the study: names of proteins, number of identified peptides, p-values, fold changes, effect size for all group comparisons, and UniProt accession numbers (XLSX)

Table S6, results of Pearson's correlation analyses between the DEPs identified in CKD5 vs CVD2 comparison (XLSX)

Table S7: A detailed list of IPA annotation results for canonical pathway, diseases/functions and upstream regulator categories with $-\log_{10}$ B−H corrected p-values and *z*-scores (XLSX)

https://doi.org/10.1021/acs.jproteome.0c00883
J. Proteome Res. 2021, 20, 3053−3067

AUTHOR INFORMATION

Corresponding Author

Magdalena Luczak − *Institute of Bioorganic Chemistry, Polish Academy of Sciences, 61-704 Poznan, Poland;* orcid.org/0000-0002-2182-5699; Email: magdalu@ibch.poznan.pl

Authors

Joanna Tracz − *Institute of Bioorganic Chemistry, Polish Academy of Sciences, 61-704 Poznan, Poland;* orcid.org/0000-0003-0962-5114

Luiza Handschuh − *Institute of Bioorganic Chemistry, Polish Academy of Sciences, 61-704 Poznan, Poland*

Maciej Lalowski − *Institute of Bioorganic Chemistry, Polish Academy of Sciences, 61-704 Poznan, Poland; Helsinki Institute for Life Science (HiLIFE) and Faculty of Medicine, Biochemistry/Developmental Biology, Meilahti Clinical Proteomics Core Facility, University of Helsinki, 00100 Helsinki, Finland*

Łukasz Marczak − *Institute of Bioorganic Chemistry, Polish Academy of Sciences, 61-704 Poznan, Poland;* orcid.org/0000-0001-8602-0077

Katarzyna Kostka-Jeziorny − *Department of Hypertension, Angiology and Internal Disease, Poznan University of Medical Sciences, 61-848 Poznan, Poland*

Bartłomiej Perek − *Department of Cardiac Surgery and Transplantology, Poznan University of Medical Sciences, 61-848 Poznan, Poland*

Maria Wanic-Kossowska − *Department of Nephrology, Transplantology and Internal Medicine, Poznan University of Medical Sciences, 60-355 Poznan, Poland*

Alina Podkowińska − *Dialysis Station Dravis sp. z o.o., 60-631 Poznan, Poland*

Andrzej Tykarski − *Department of Hypertension, Angiology and Internal Disease, Poznan University of Medical Sciences, 61-848 Poznan, Poland*

Dorota Formanowicz − *Department of Medical Chemistry and Laboratory Medicine, Poznan University of Medical Sciences, 60-806 Poznan, Poland*

Complete contact information is available at: https://pubs.acs.org/10.1021/acs.jproteome.0c00883

Author Contributions

J. Tracz: investigation, validation, writing - original draft; L. Handschuh, L. Marczak: investigation; M. Lalowski: formal analysis, writing - review and editing; K. Kostka-Jeziorny, B. Perek, A. Podkowińska, A. Tykarski and M. Wanic-Kossowska: resources; D. Formanowicz: conceptualization, resources, writing - review and editing; M. Luczak: conceptualization, formal analysis, visualization, writing - review and editing, supervision, funding acquisition. All authors read and approved the final version of a manuscript.

Notes

The authors declare no competing financial interest.

ACKNOWLEDGMENTS

This work was supported by the National Science Centre, Poland, under grant no. 2015/19/B/NZ2/02450, to M. Luczak. The authors wish to thank Dr. Agnieszka Fedoruk-Wyszomirska and Dr. Dorota Gurda (Institute of Bioorganic Chemistry PAS) for support in confocal microscopy and flow cytometry. The graphical abstract was generated using the web-based tool BioRender (Biorender.com).

REFERENCES

(1) Levin, A.; Stevens, P. E.; Bilous, R. W.; Coresh, J.; De Francisco, A. L. M.; De Jong, P. E.; Griffith, K. E.; Hemmelgarn, B. R.; Iseki, K.; Lamb, E. J.; Levey, A. S.; Riella, M. C.; Shlipak, M. G.; Wang, H.; White, C. T.; Winearls, C. G. Kidney Disease: Improving Global Outcomes (KDIGO) CKD Work Group. KDIGO 2012 Clinical Practice Guideline for the Evaluation and Management of Chronic Kidney Disease. *Kidney Int. Suppl.* **2013**, *3*, 1−150.

(2) Gansevoort, R. T.; Correa-Rotter, R.; Hemmelgarn, B. R.; Jafar, T. H.; Heerspink, H. J. L.; Mann, J. F.; Matsushita, K.; Wen, C. P. Chronic Kidney Disease and Cardiovascular Risk: Epidemiology, Mechanisms, and Prevention. *Lancet* **2013**, *382*, 339−352.

(3) Go, A. S.; Chertow, G. M.; Fan, D.; McCulloch, C. E.; Hsu, C. Y. Chronic Kidney Disease and the Risks of Death, Cardiovascular Events, and Hospitalization. *N. Engl. J. Med.* **2004**, *351* (13), 1296−1305.

(4) De Jager, D. J.; Grootendorst, D. C.; Jager, K. J.; Van Dijk, P. C.; Tomas, L. M. J.; Ansell, D.; Collart, F.; Finne, P.; Heaf, J. G.; De Meester, J.; Wetzels, J. F. M.; Rosendaal, F. R.; Dekker, F. W. Cardiovascular and Noncardiovascular Mortality among Patients Starting Dialysis. *JAMA - J. Am. Med. Assoc.* **2009**, *302* (16), 1782−1789.

(5) Van Der Velde, M.; Matsushita, K.; Coresh, J.; Astor, B. C.; Woodward, M.; Levey, A.; De Jong, P.; Gansevoort, R. T.; El-Nahas, M.; Eckardt, K. U.; Kasiske, B. L.; Ninomiya, T.; Chalmers, J.; MacMahon, S.; Tonelli, M.; Hemmelgarn, B.; Sacks, F.; Curhan, G.; Collins, A. J.; Li, S.; Chen, S. C.; Hawaii Cohort, K. P.; Lee, B. J.; Ishani, A.; Neaton, J.; Svendsen, K.; Mann, J. F. E.; Yusuf, S.; Teo, K. K.; Gao, P.; Nelson, R. G.; Knowler, W. C.; Bilo, H. J.; Joosten, H.; Kleefstra, N.; Groenier, K. H.; Auguste, P.; Veldhuis, K.; Wang, Y.; Camarata, L.; Thomas, B.; Manley, T. Lower Estimated Glomerular Filtration Rate and Higher Albuminuria Are Associated with All-Cause and Cardiovascular Mortality. A Collaborative Meta-Analysis of High-Risk Population Cohorts. *Kidney Int.* **2011**, *79* (12), 1341−1352.

(6) Kalantar-Zadeh, K.; Block, G.; Humphreys, M. H.; Kopple, J. D. Reverse Epidemiology of Cardiovascular Risk Factors in Maintenance Dialysis Patients. *Kidney Int.* **2003**, *63*, 793−808.

(7) Maini, R.; Wong, D. B.; Addison, D.; Chiang, E.; Weisbord, S. D.; Jneid, H. Persistent Underrepresentation of Kidney Disease in Randomized, Controlled Trials of Cardiovascular Disease in the Contemporary Era. *J. Am. Soc. Nephrol.* **2018**, *29* (12), 2782−2786.

(8) Podkowińska, A.; Formanowicz, D. Chronic Kidney Disease as Oxidative Stress- and Inflammatory-Mediated Cardiovascular Disease. *Antioxidants* **2020**, *9* (8), 752.

(9) Romanova, Y.; Laikov, A.; Markelova, M.; Khadiullina, R.; Makseev, A.; Hasanova, M.; Rizvanov, A.; Khaiboullina, S.; Salafutdinov, I. Proteomic Analysis of Human Serum from Patients with Chronic Kidney Disease. *Biomolecules* **2020**, *10* (2), 257.

(10) Lygirou, V.; Latosinska, A.; Makridakis, M.; Mullen, W.; Delles, C.; Schanstra, J. P.; Zoidakis, J.; Pieske, B.; Mischak, H.; Vlahou, A. Plasma Proteomic Analysis Reveals Altered Protein Abundances in Cardiovascular Disease. *J. Transl. Med.* **2018**, *16* (1), 104.

(11) Luczak, M.; Suszynska-Zajczyk, J.; Marczak, L.; Formanowicz, D.; Pawliczak, E.; Wanic-Kossowska, M.; Stobiecki, M. Label-Free Quantitative Proteomics Reveals Differences in Molecular Mechanism of Atherosclerosis Related and Non-Related to Chronic Kidney Disease. *Int. J. Mol. Sci.* **2016**, *17*, 631.

(12) *Chronic Kidney Disease (Partial Update): Early Identification and Management of Chronic Kidney Disease in Adults in Primary and Secondary Care*, NICE Clinical Guidelines, No. 182; National Institute for Health and Care Excellence: London, UK, 2014.

(13) Levey, A. S.; Bosch, J. P.; Lewis, J. B.; Greene, T.; Rogers, N.; Roth, D. A More Accurate Method to Estimate Glomerular Filtration Rate from Serum Creatinine: A New Prediction Equation.

Modification of Diet in Renal Disease Study Group. *Ann. Intern. Med.* **1999**, *130* (6), 461−470.
(14) Dagur, P. K.; McCoy, J. P. Collection, Storage, and Preparation of Human Blood Cells. *Curr. Protoc. Cytom.* **2015**, *73*, 5.1.1−5.1.16.
(15) Cox, J.; Mann, M. MaxQuant Enables High Peptide Identification Rates, Individualized p.p.b.-Range Mass Accuracies and Proteome-Wide Protein Quantification. *Nat. Biotechnol.* **2008**, *26* (12), 1367−1372.
(16) Handschuh, L.; Wojciechowski, P.; Kazmierczak, M.; Marcinkowska-Swojak, M.; Luczak, M.; Lewandowski, K.; Komarnicki, M.; Blazewicz, J.; Figlerowicz, M.; Kozlowski, P. NPM1 Alternative Transcripts Are Upregulated in Acute Myeloid and Lymphoblastic Leukemia and Their Expression Level Affects Patient Outcome. *J. Transl. Med.* **2018**, *16*, 232.
(17) MacLean, B.; Tomazela, D. M.; Shulman, N.; Chambers, M.; Finney, G. L.; Frewen, B.; Kern, R.; Tabb, D. L.; Liebler, D. C.; MacCoss, M. J. Skyline: An Open Source Document Editor for Creating and Analyzing Targeted Proteomics Experiments. *Bioinformatics* **2010**, *26* (7), 966−968.
(18) Levin, Y. The Role of Statistical Power Analysis in Quantitative Proteomics. *Proteomics* **2011**, *11* (12), 2565−2567.
(19) Cohen, J. A Power Primer. *Psychol. Bull.* **1992**, *112* (1), 155−159.
(20) Hedges, L. V.; Olkin, I. *Statistical Methods for Meta-Analysis*; Academic Press, 1985.
(21) Pezzini, F.; Bianchi, M.; Benfatto, S.; Griggio, F.; Doccini, S.; Carrozzo, R.; Dapkunas, A.; Delledonne, M.; Santorelli, F. M.; Lalowski, M. M.; Simonati, A. The Networks of Genes Encoding Palmitoylated Proteins in Axonal and Synaptic Compartments Are Affected in PPT1 Overexpressing Neuronal-like Cells. *Front. Mol. Neurosci.* **2017**, *10*, 266.
(22) Rossi, E.; Lopez-Novoa, J. M.; Bernabeu, C. Endoglin Involvement 1 in Integrin-Mediated Cell Adhesion as a Putative Pathogenic Mechanism in Hereditary Hemorrhagic Telangectasia Type 1 (HHT1). *Front. Genet.* **2015**, *5*, 457.
(23) Muntner, P.; He, J.; Astor, B. C.; Folsom, A. R.; Coresh, J. Traditional and Nontraditional Risk Factors Predict Coronary Heart Disease in Chronic Kidney Disease: Results from the Atherosclerosis Risk in Communities Study. *J. Am. Soc. Nephrol.* **2005**, *16* (2), 529−538.
(24) Recio-Mayoral, A.; Banerjee, D.; Streather, C.; Kaski, J. C. Endothelial Dysfunction, Inflammation and Atherosclerosis in Chronic Kidney Disease − a Cross-Sectional Study of Predialysis, Dialysis and Kidney-Transplantation Patients. *Atherosclerosis* **2011**, *216* (2), 446−451.
(25) Woollard, K. J.; Geissmann, F. Monocytes in Atherosclerosis: Subsets and Functions. *Nat. Rev. Cardiol.* **2010**, *7* (2), 77−86.
(26) Schwarz, U.; Buzello, M.; Ritz, E.; Stein, G.; Raabe, G.; Wiest, G.; Mall, G.; Amann, K. Morphology of Coronary Atherosclerotic Lesions in Patients with End- Stage Renal Failure Patients and Age and Sex Matched Non-Uraemic. *Nephrol., Dial., Transplant.* **2000**, *15*, 218−223.
(27) Campean, V.; Neureiter, D.; Varga, I.; Runk, F.; Reiman, A.; Garlichs, C.; Achenbach, S.; Nonnast-Daniel, B.; Amann, K. Atherosclerosis and Vascular Calcification in Chronic Renal Failure. *Kidney Blood Pressure Res.* **2006**, *28* (5−6), 280−289.
(28) Bowe, B.; Xie, Y.; Xian, H.; Li, T.; Al-Aly, Z. Association between Monocyte Count and Risk of Incident CKD and Progression to ESRD. *Clin. J. Am. Soc. Nephrol.* **2017**, *12* (4), 603−613.
(29) Luczak, M.; Formanowicz, D.; Marczak, Ł.; Suszyńska-Zajczyk, J.; Pawliczak, E.; Wanic-Kossowska, M.; Stobiecki, M. ITRAQ-Based Proteomic Analysis of Plasma Reveals Abnormalities in Lipid Metabolism Proteins in Chronic Kidney Disease-Related Atherosclerosis. *Sci. Rep.* **2016**, *6*, 32511.
(30) Heemskerk, N.; Van Rijssel, J.; Van Buul, J. D. Rho-GTPase Signaling in Leukocyte Extravasation: An Endothelial Point of View. *Cell Adhesion and Migration.* **2014**, *8* (2), 67−75.
(31) Finney, A. C.; Stokes, K. Y.; Pattillo, C. B.; Orr, A. W. Integrin Signaling in Atherosclerosis. *Cell. Mol. Life Sci.* **2017**, *74* (12), 2263−2282.
(32) Davies, M. J.; Gordon, J. L.; Gearing, A. J. H.; Pigott, R.; Woolf, N.; Katz, D.; Kyriakopoulos, A. The Expression of the Adhesion Molecules ICAM-1, VCAM-1, PECAM, and E-Selectin in Human Atherosclerosis. *J. Pathol.* **1993**, *171* (3), 223−229.
(33) Gross, M. D.; Bielinski, S. J.; Suarez-Lopez, J. R.; Reiner, A. P.; Bailey, K.; Thyagarajan, B.; Carr, J. J.; Duprez, D. A.; Jacobs, D. R., Jr. Circulating Soluble Intercellular Adhesion Molecule 1 and Subclinical Atherosclerosis: The Coronary Artery Risk Development in Young Adults Study. *Clin. Chem.* **2012**, *58* (2), 411−420.
(34) Luc, G.; Arveiler, D.; Evans, A.; Amouyel, P.; Ferrieres, J.; Bard, J.-M.; Elkhalil, L.; Fruchart, J.-C.; Ducimetiere, P. Circulating Soluble Adhesion Molecules ICAM-1 and VCAM-1 and Incident Coronary Heart Disease: The PRIME Study. *Atherosclerosis* **2003**, *170* (1), 169−176.
(35) Hepper, I.; Schymeinsky, J.; Weckbach, L. T.; Jakob, S. M.; Frommhold, D.; Sixt, M.; Laschinger, M.; Sperandio, M.; Walzog, B. The Mammalian Actin-Binding Protein 1 Is Critical for Spreading and Intraluminal Crawling of Neutrophils under Flow Conditions. *J. Immunol.* **2012**, *188* (9), 4590−4601.
(36) Phillipson, M.; Heit, B.; Colarusso, P.; Liu, L.; Ballantyne, C. M.; Kubes, P. Intraluminal Crawling of Neutrophils to Emigration Sites: A Molecularly Distinct Process from Adhesion in the Recruitment Cascade. *J. Exp. Med.* **2006**, *203* (12), 2569−2575.
(37) Rossi, E.; Bernabeu, C.; Smadja, D. M. Endoglin as an Adhesion Molecule in Mature and Progenitor Endothelial Cells: A Function beyond TGF-β. *Front. Med.* **2019**, *6*, 10.
(38) Rossi, E.; Sanz-Rodriguez, F.; Eleno, N.; Düwell, A.; Blanco, F. J.; Langa, C.; Botella, L. M.; Cabañas, C.; Lopez-Novoa, J. M.; Bernabeu, C. Endothelial Endoglin Is Involved in Inflammation: Role in Leukocyte Adhesion and Transmigration. *Blood* **2013**, *121* (2), 403−415.
(39) Alon, R.; Feigelson, S. W.; Manevich, E.; Rose, D. M.; Schmitz, J.; Overby, D. R.; Winter, E.; Grabovsky, V.; Shinder, V.; Matthews, B. D.; Sokolovsky-Eisenberg, M.; Ingber, D. E.; Benoit, M.; Ginsberg, M. H. A4β1-Dependent Adhesion Strengthening under Mechanical Strain Is Regulated by Paxillin Association with the A4-Cytoplasmic Domain. *J. Cell Biol.* **2005**, *171* (6), 1073−1084.
(40) Rullo, J.; Becker, H.; Hyduk, S. J.; Wong, J. C.; Digby, G.; Arora, P. D.; Cano, A. P.; Hartwig, J.; McCulloch, C. A.; Cybulsky, M. I. Actin Polymerization Stabilizes A4β1 Integrin Anchors That Mediate Monocyte Adhesion. *J. Cell Biol.* **2012**, *197* (1), 115−129.
(41) Lee, A.; Whyte, M. K. B.; Haslett, C. Inhibition of Apoptosis and Prolongation of Neutrophil Functional Longevity by Inflammatory Mediators. *J. Leukocyte Biol.* **1993**, *54*, 283−288.
(42) Whyte, M. K.; Meagher, L. C.; MacDermot, J.; Haslett, C. Impairment of Function in Aging Neutrophils Is Associated with Apoptosis. *J. Immunol.* **1993**, *150* (11), 5124−5134.
(43) Modaresi, A.; Nafar, M.; Sahraei, Z. Oxidative Stress in Chronic Kidney Disease. *Iran. J. Kidney Dis.* **2015**, *9* (3), 165−179.

https://doi.org/10.1021/acs.jproteome.0c00883
J. Proteome Res. 2021, 20, 3053−3067